Stability and Dynamics of the Porcine Odorant-Binding Protein[†]

Maria Staiano,[‡] Sabato D'Auria,*[,‡] Antonio Varriale,[‡] Mose' Rossi,[‡] Anna Marabotti,[§] Carlo Fini,[||] Olesya V. Stepanenko,[⊥] Irina M. Kuznetsova,[⊥] and Konstantin K. Turoverov*[,⊥]

Institute of Protein Biochemistry, CNR, Naples, Italy, Institute of Food Sciences, CNR, Avellino, Italy, University of Perugia, Italy, and Institute of Cytology, RAS, St. Petersburg, Russia

Received April 29, 2007; Revised Manuscript Received July 24, 2007

ABSTRACT: The denaturation process of porcine odorant-binding protein (pOBP) was studied by intrinsic fluorescence analysis and far- and near-UV circular dichroism measurements. Our results showed that a reversible one-step process described the denaturation by GdnHCl. The midpoint of the transition, that is, the point where the free energies of protein in the native and unfolded states are equal, corresponds to 2.3 M GdnHCl. The difference in free energy between native and unfolded states of pOBP is −5.95 kcal/mol in the absence of GdnHCl, indicating that the protein molecule is very stable to the denaturing action of GdnHCl. A 15% increase in fluorescence intensity accompanied by a 25% decrease of fluorescence decay lifetime recorded in the range of 0.0−1.4 M GdnHCl was explained by the destruction of the complex between Trp 16 and the positively charged atom NZ of Lys 120, localized over the center of the Trp 16 indole ring, with concurrent formation of complex between Trp 16 and bound water molecules also located in its close vicinity.

Lipocalins are proteins expressed in animals and plants as well as in bacteria. Despite their low sequence identity (less than 20%), they present a conserved structural frame named "lipocalin fold" made up of two domains: an eight-strand β-barrel connected by a short linker (hinge sequence) to a C-terminal α-helix (*1*). The β-barrel contains 70−80% of the total amino acid residues, and it contains the ligand-binding site. The function of the α-helix is not currently known (*1*).

During the evolutionary pathway, the structural frame of lipocalins gave rise to a large variety of scaffolds, defined as structural frames that can acquire new binding specificities when subjected to molecular engineering programs (*2*). Protein scaffolds can be used for the production of affinity innovative biosensors for small molecules sensing. In fact, it is known that protein scaffolds are composed of stable frames that do not modify their overall 3-D organization in response to multiple changes in their amino acid sequence (*2*).

Lipocalins have already been subjected to molecular engineering programs that have highlighted their use as protein scaffolds for the development of affinity reagents (*3*, *4*). To this regard, the binding specificity of bilin-binding protein, an insect lipocalin, has been optimized for the binding of digoxigenin, a molecule of relevant biotechnological interest with structural and chemical physical properties totally different from those of biliverdin, the natural ligand of the native protein (*5*). Since explosive compounds have usually a molecular mass and chemical properties comparable to those of lipocalins' natural ligands, it should not be outrageous to propose the use of these proteins as probe for optical biosensors for the specific detection of explosive substances. In this respect, it would be worthy to investigate from a thermodynamic point of view the structural stability and the conformational dynamics of lipocalins.

Odorant-binding proteins (OBP) are a subclass of the lipocalin family with the ability to bind reversibly odorant molecules, which commonly are volatile, small and hydrophobic compounds with no fixed structure and chemical properties (*6*). In this family, the first 3D structure resolved was that of bovine OBP, which turned out to be a dimer with a peculiar structure formed by the swapping of two domains each belonging to the other subunit (*7*, *8*). The absence of a disulfide bridge that, in contrast, is present in all of the members of the lipocalin families was also evident (*6*). Despite its rather high sequence identity (42%) with bovine OBP, the crystallographic structure of porcine OBP (pOBP[1]) determined at 2.25 Å resolution (*9*) confirmed that pOBP is a monomeric protein of 20 kDa, showing the

[†] This work was partially supported by NATO Project PST.NR.CLG 981025 (S.D., K.K.T.), Program MCB RAS, Program "Leading Scientific Schools of Russia" #9396.2006.4, FASI Contract #02.512.11. 2108 (K.K.T.), CNR-NATO Project 215.36S, Russian Science Support Foundation, RFBR 06-04-48231 and Grant of St. Petersburg administration for post-graduate students and young scientists (O.S.), ISA-CNR by CNR-Bioinformatics Project (A.M.), and also by the CNR Commessa Diagnostica avanzata ed alimentazione (S.D., M.S.).

* To whom correspondence should be addressed. S.D.: Institute of Protein Biochemistry CNR, Via Pietro Castellino, 111 80131 Napoli, Italy; tel, +39-0816132250; fax, +39-0816132277; e-mail, s.dauria@ibp.cnr.it. K.K.T.: Institute of Cytology Russian Academy of Sciences, Tikhoretsky av., 4, St. Petersburg, Russia; tel, +7-8122971957; fax, +7-8122970341; e-mail, kkt@mail.cytspb.rssi.ru.

[‡] Institute of Protein Biochemistry, CNR.

[§] Institute of Food Sciences, CNR.

[||] University of Perugia.

[⊥] Institute of Cytology, RAS.

[1] Abbreviations: pOBP, porcine odorant-binding protein; GdnHCl, guanidine hydrochloride; CD, circular dichroism; UV, ultraviolet; parameter *A*, (I_{320}/I_{365}) upon excitation at $\lambda_{ex} = 297$ nm; MD, molecular dynamics.

10.1021/bi7008129 CCC: $37.00
Published on Web 09/11/2007

β-barrel structure common to the lipocalin family formed by nine strands, with an additional helical domain between residues 124 and 141. The β-barrel structure shows a high content of hydrophobic and aromatic amino acid side chains forming a big cluster at the protein core and, in particular, they set up the internal cavity of the β-barrel itself (*9*). The conserved disulfide bridge between Cys 63 and Cys 155 links the C-terminal moiety to the strand β4.

In this work we used steady-state and time-resolved fluorescence spectroscopy as well as circular dichroism experiments to investigate the structural stability and the conformational dynamics of pOBP.

MATERIALS AND METHODS

Protein Purification. Pig (*Sus scrofa*, breed Large White) nasal mucosa was obtained from the local slaughterhouse. The tissue was collected within 20 min after death and quickly utilized for the extraction of pOBP. Protein was purified from fresh porcine nasal tissue according to the procedure described by Dal Monte et al. (*10*). This procedure yielded on average 15 mg of purified pOBP-I from a single animal. GdnHCl (Nacalai Tesque, Japan) was used without additional purification. The GdnHCl concentration was determined by refraction index with an Abbe refractometer (LOMO, Russia).

Fluorescence Measurements. Fluorescence experiments were carried out using a homemade spectrofluorimeter with steady-state and time-resolved excitation (*11*). Fluorescence was excited at the long-wave absorption spectrum edge (297 nm), where the contribution of tyrosine residues in the bulk protein fluorescence is negligible, and at 280 nm where both tyrosine and tryptophan residues absorb. The position and form of the fluorescence spectra were characterized by the parameter $A = (I_{320}/I_{365})_{297}$, where I_{320} and I_{365} are fluorescence intensities at $\lambda_{em} = 320$ and 365 nm, respectively, and $\lambda_{ex} = 297$ nm (*12*). The values of parameter A and of fluorescence spectrum were corrected by the instrument sensitivity.

Analysis of the Fluorescence Decay. To analyze the decay curves a special program was used (*11*). The fitting routine was based on the nonlinear least-squares method. Minimization was accomplished according to Marquardt (*13*). Experimental data were analyzed using the multiexponential approach:

$$I(t) = \sum_i \alpha_i \exp(-t/\tau_i) \tag{1}$$

where α_i and τ_i are amplitude and lifetime of component i, $\sum\alpha_i = 1$.

The contribution of component i to the total emission S_i was calculated as

$$S_i = \frac{\alpha_i \int_0^\infty \exp(-t/\tau_i)\, dt}{\sum \alpha_i \int_0^\infty \exp(-t/\tau_i)\, dt} = \frac{\alpha_i \tau_i}{\sum \alpha_i \tau_i} \tag{2}$$

The root-mean-square value of fluorescent lifetimes, $\langle\tau\rangle$, for biexponential decay is determined as

$$\langle\tau\rangle = \frac{\alpha_1 {\tau_1}^2 + \alpha_2 {\tau_2}^2}{\alpha_1 \tau_1 + \alpha_2 \tau_2} \tag{3}$$

Stern−Volmer Quenching and Estimation of the Bimolecular Quenching Rates. The conformational state of proteins was further characterized by acrylamide-induced fluorescence quenching. Experiments were performed using excitation at 297 nm with fluorescence emission set at 360 nm. Quenching data were plotted as the ratio of fluorescence in the absence of quencher (I_0) to the intensity in the presence of quencher (I) against quencher concentration. The resulting data were fit to dynamic parameters according to the Stern−Volmer equation $I_0/I = 1 + K_{SV}[Q]$, where K_{SV} is the Stern−Volmer quenching constant and [Q] the quencher concentration (*14*).

Circular Dichroism Measurements. CD spectra were obtained with a Jasco-810 spectrophotometer (Jasco, Japan), using a protein concentration of 0.5 mg/mL for far-UV CD measurements. Far-UV CD spectra were recorded in a 1 mm path length cell from 250 to 190 nm with a step size of 0.1 nm, a bandwidth of 1.0 nm, and an averaging time of 4 s. Near-UV CD spectra were recorded in a 1.0 cm path length cell from 400 to 250 nm with a step size of 1.0 nm, a bandwidth of 1.5 nm, and an averaging time of 10 s. For all spectra, an average of 5 scans was obtained. CD spectra of the appropriate buffers were recorded and subtracted from the protein spectra.

Analysis of Protein 3D Structure. The location of tryptophan and tyrosine residues in pOBP was analyzed according to the atomic coordinates of the crystal structure of pOBP (1A3Y.pdb, (*9*)) available from the PDB database (*15*). The microenvironment of the tryptophan or tyrosine residue was determined as a set of atoms located at a distance less than r_0 from the geometrical center of the indole or phenol ring; r_0 was taken equal to 7 Å (*16*, *17*). The nearest atom in the microenvironment to each atom of the indole or phenol ring was specified, and the distance between them was determined. For tyrosine residues the neighbors of the OH group were also determined. The packing density of the atoms in a microenvironment was determined as the number of atoms comprising the microenvironment, or as the part of microenvironment volume (V_0) occupied by the atoms ($d = \sum V_i/V_0$). The volume occupied by each atom (V_i) was determined according to its van der Waals radius, and only the part inside the microenvironment was taken into account. The real values of atom volume are slightly smaller, as atoms are incorporated in chemical bonds. Nonetheless, this was found to be not significant for the estimation of microenvironment packing density of tryptophan and tyrosine residues.

The efficiency of nonradiative energy transfer between any two chromophores was evaluated as follows (*18*):

$$W = \frac{1}{1 + \frac{2/3}{k^2}\left(\frac{R}{R_0}\right)^6} \tag{4}$$

Here R_0 is Förster distance, *i.e.*, the averaged distance between randomly orientated donor and acceptor at which $W = 0.5$; R is the distance between the geometrical centers of the indole (or phenol) rings of a donor and an acceptor; and k^2 is the factor of mutual orientation of the donor and the acceptor:

$$k^2 = (\cos\theta - 3\cos\theta_A \cos\theta_D)^2 \tag{5}$$

where θ is the angle between the directions of the emission oscillator of a donor and the absorption oscillator of an acceptor; θ_D is the angle between the direction of emission oscillator and the vector connecting the geometrical center of the donor, and θ_A is the angle between the direction of absorption oscillator and the vector connecting the geometrical center of the acceptor (*19*). The values of R_0 for Tyr−Trp and Tyr−Tyr pairs were taken from ref *20*. All other parameters were determined according to atoms coordinates. Oscillators were considered to be rigid in all calculations.

Molecular Dynamics Simulations. The file 1A3Y.pdb (*9*) was also used as a starting point to perform molecular dynamics (MD) simulations of pOBP in water. The file was edited to remove monomer B present in the crystal and the coordinates of Pro 9 (the first residue in the structure), which were not complete. Simulations were carried out using the program GROMACS version 3.3.1 (*21*, *22*), running in parallel on a cluster with x86_64 architecture, with operating system Linux CENTOS version 4.2, based on kernel 2.6.9-22. The OPLS-AA force field (*23*, *24*) was used throughout the simulations. A cubic box, containing approximately 6500 water molecules (SPC model) (*25*) and 16 Na^+ ions to neutralize the net negative charge of the protein, was used to solvate pOBP. Periodic boundary conditions were applied to eliminate surface effects. A preliminary energy minimization with a tolerance of 1000 kJ/mol/nm was applied using the steepest descent method. All bonds were constrained using LINCS (*26*). After minimization, the system was submitted to a short MD simulation (20 ps) with position restraints to better "soak" the water molecules into the macromolecule, with a time step of 2 fs and coupling the system to a temperature bath at 300 K using Berendsen's method (*27*). Berendsen's pressure coupling was also used. Long-range electrostatics were handled using the PME method (*28*). Cutoffs were set at 0.9 nm for Coulomb interactions and at 1.4 nm for van der Waals interactions. The final MD simulation was carried out at 300 K for 500 ps, with a time step of 2 fs and without any position restraints. Analysis of the distances between atoms and calculation of dihedral angles during the trajectory was carried out with the program VMD (*29*).

RESULTS AND DISCUSSION

pOBP Unfolding by GdnHCl Recorded by Intrinsic Fluorescence and CD Spectra. The conformational changes induced by GdnHCl on pOBP were explored by fluorescence spectroscopy and far- and near-UV CD spectral analysis. Intrinsic fluorescence emission intensity at 320 and 365 nm as a function of GdnHCl concentration is shown in Figure 1A. The variation of the parameter $A = I_{320}/I_{365}$, characterizing the fluorescence spectrum position, is plotted in Figure 1B. Intrinsic fluorescence emission spectra excited at 297 and 280 nm are reported in Figure 2A and Figure 2B, respectively; in addition, Figure 2C represents their difference spectra characterizing the contribution of tyrosine residues to the global fluorescence of the protein.

The fluorescence intensity decay for native and unfolded pOBP is given in Figure 3. The variation of the tryptophan residue excited-state lifetime, fluorescence anisotropy, and far-UV CD data with the change of GdnHCl concentration are presented in Figure 1 panels A, C, and D. Figure 4 shows

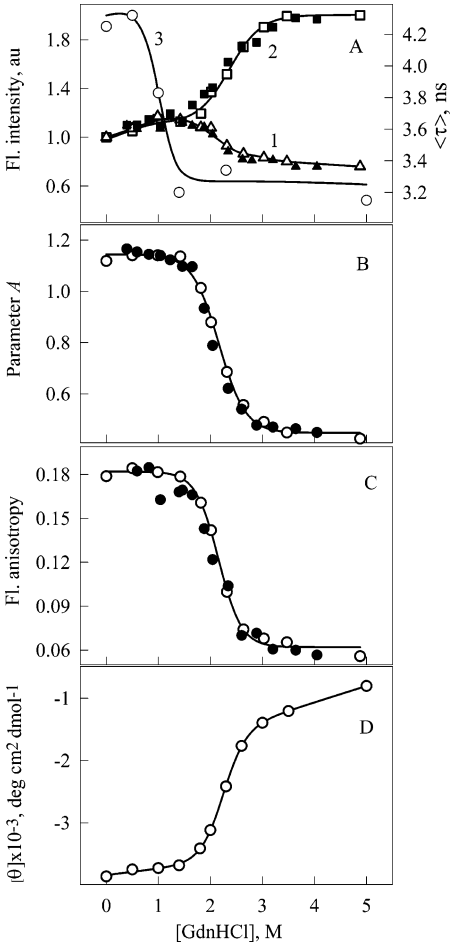

FIGURE 1: GdnHCl induced conformational transitions of pOBP. (A) The change of the fluorescence intensity recorded at 320 nm (1) and at 365 nm (2) and the lifetime of fluorescence (3). (B) The change of the parameter $A = I_{320}/I_{365}$. (C) The change of fluorescence anisotropy at 365 nm. (D) The change of ellipticity at 222 nm. Unfolding and refolding are presented by open and closed symbols, respectively. $\lambda_{ex} = 297$ nm.

far- and near-UV CD spectra in different concentrations of GdnHCl. All in all the obtained results allowed distinguishing three subranges of GdnHCl concentrations 0−1.4, 1.4−3.5, and 3.5−5.0 M which are worth examining separately.

A small amount of GdnHCl (0−1.4 M) causes only local disturbance of the pOBP structure, recorded by the increase of ellipticity in near-UV (Figure 4, inset) and changes of fluorescence intensity and lifetime of fluorescence decay (Figure 1A). It is interesting that along with the increase of fluorescence intensity the fluorescence lifetime decreases to the value typical for unfolded proteins (*30*). Earlier we have shown that such amounts of GdnHCl change the slope of temperature dependence of parameter *A* in the temperature range preceding heating denaturation (*31*). All the other parameters, namely, fluorescence spectrum position, fluorescence anisotropy, and far-UV CD spectra, remained constant in this first subrange of GdnHCl. The accessibility of Trp 16 to the solvent (Figure 5) and the contribution of tyrosine residues to the bulk protein fluorescence remain also unchanged (Figure 2C).

Apparently, the unfolding of protein structure occurred in the range of GdnHCl concentrations 1.4 to 3.5 M. This process was accompanied by dramatic changes of practically all recorded parameters. Fluorescence intensity measured at

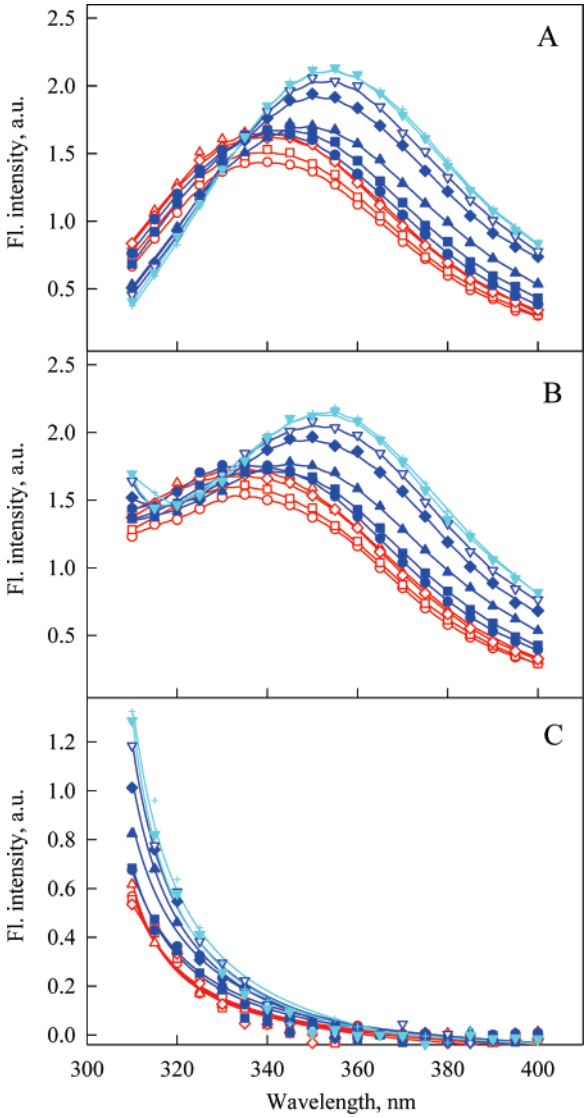

FIGURE 2: Emission spectrum of intrinsic fluorescence recorded at 297 nm (panel A) and 280 nm (panel B). The difference between the fluorescence spectra excited at 280 and 297 nm (panel C) represents the contribution of the Tyr residues to the bulk fluorescence of the protein. The protein solutions contain 0.0, 0.5, 1.0, 1.4, 1.8, 2.0, 2.3, 2.6, 3.0, 3.5, 5.0 M GdnHCl. Data corresponding to three subranges of GdnHCl concentrations, 0−1.4, 1.4−3.5, and 3.5−5.0 M, are colored in red, dark blue, and blue, respectively.

320 nm decreases from 1.17 to 0.8, whereas fluorescence intensity recorded at 365 nm rose from 1.14 to 1.99 (Figure 1A). In agreement with these changes, the value of parameter *A* diminished from 1.14 to 0.45, *i.e.*, to a value that is typical for completely unfolded proteins. The decrease of parameter *A* reveals the red shift of protein fluorescence spectra (Figure 2) common with protein unfolding. As is typical for proteins, pOBP unfolding is accompanied by a decrease of fluorescence anisotropy (Figure 1C), indicating an increase of intramolecular mobility with destruction of tertiary structure, and by a decrease of ellipticity at 222 nm (Figures 1D and 4), indicating violation of protein secondary structure. Here, the only exception was represented by the fact that pOBP has a low fluorescence lifetime in 1.4 M, which remained constant instead of decreasing as usual during protein unfolding. The parametric dependence (*32*) between I_{320} and I_{365} (Figure 6) also proved the existence of two significantly

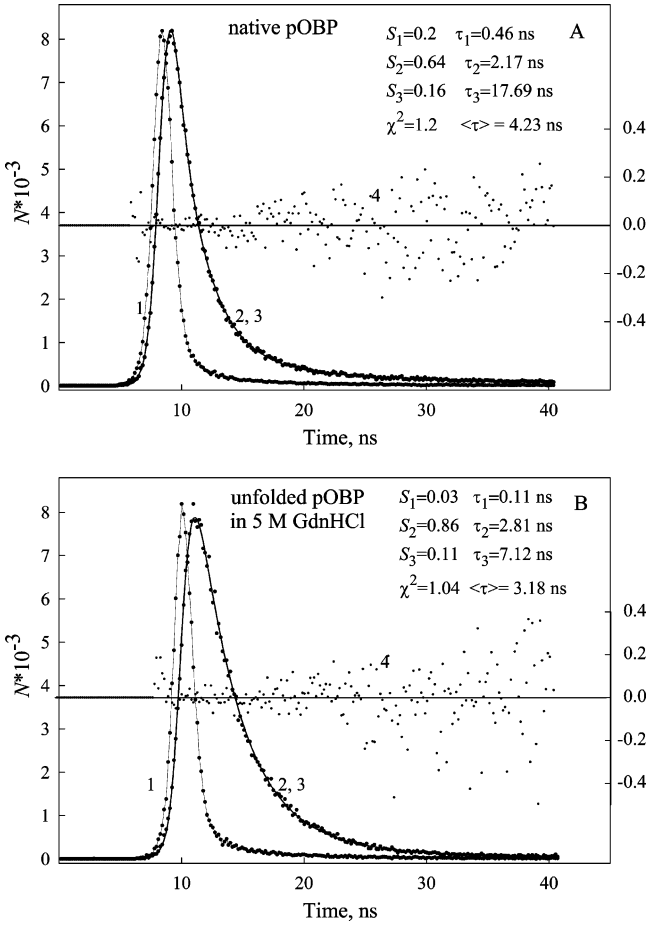

FIGURE 3: Decay curves of tryptophan fluorescence of native (A) and unfolded (B) pOBP. Figures represent excitation lamp profile (curve 1), experimental decay curve (curve 2), best-fitting calculated fluorescence decay curve (curve 3), and deviation between the experimental and calculated decay curve (weighted residuals; curve 4). λ_{ex} = 297 nm, λ_{reg} = 365 nm. The fluorescence decay curves show the best fit with a three-exponential decay model. The values of τ_i, S_i, χ^2, and average lifetime $\langle\tau\rangle$ are shown.

different processes characterizing the change of fluorescence intensity induced by GdnHCl in concentration intervals 0.0−1.4 M and 1.4−3.5 M. In the solutions containing GdnHCl over 3.5 M, pOBP is completely unfolded and further increase in GdnHCl concentrations did not induce noticeable change of the parameters recorded.

Intrinsic Tryptophan Fluorescence and Location of the Single Trp 16 in the Structure of pOBP. In order to elucidate the process taking place in the first subrange of GdnHCl concentrations, we addressed intrinsic fluorescence of pOBP. Due to its high sensitivity, convenience, and variety of information obtainable, fluorescence spectroscopy is extensively applied in investigations on proteins structure, stability, and folding. The sensitivity of tryptophan intrinsic fluorescence originates from the large variation of all of its parameters as well as from their strong dependence on its microenvironments. At the same time the theory of tryptophan fluorescence dependence upon its locations in protein could not be regarded as completed. Attempts to make generalizations allowing the identification of clear-cut classes of tryptophan residues in connection with protein structural details have failed. Apparently, the fluorescent characteristics are to a major extent individual and they reflect the individualities of their microenvironments (*17*, *33*). In other

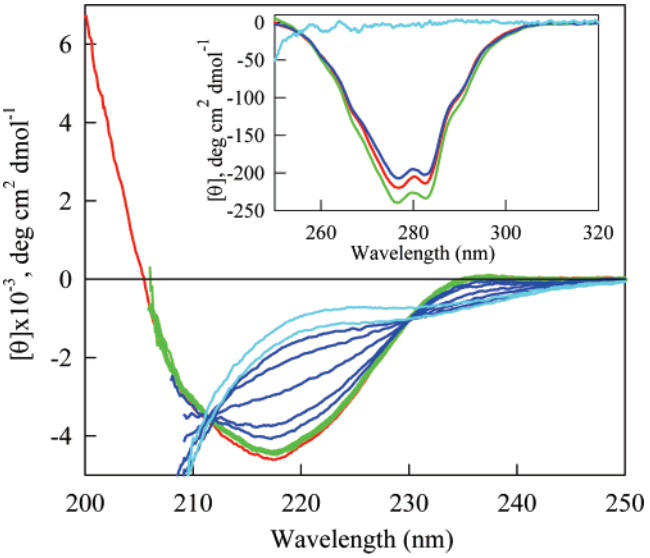

FIGURE 4: Changes of far-UV and near-UV CD of pOBP induced by GdnHCl. The far-UV CD spectra of pOBP in solutions contain 0.0, 0.5, 1.0, 1.4, 1.8, 2.0, 2.3, 2.6, 3.0, 3.5, and 5.0 M GdnHCl. Data corresponding to GdnHCl concentrations, 0, 0.5−1.4, 1.8−3.0, and 3.5−5.0 M, are showed in red, green, dark blue, and blue, respectively. Inset: The near-UV CD spectra of pOBP in solution containing 0 (red), 1.2 (green), 1.7 (dark blue), and 4.0 (blue) M.

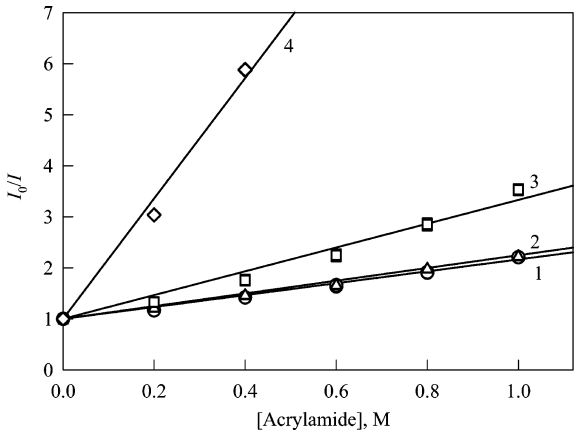

FIGURE 5: Acrylamide quenching of intrinsic fluorescence of pOBP in 0, 1.2, 1.7, and 4.0 M GdnHCl (curves 1, 2, 3, and 4).

words, any generalization can be done only on the basis of comparison of intrinsic characteristics of tryptophan residues' fluorescence with their location in protein. To this end proteins with only one tryptophan residue are most valuable. The study on pOBP unfolding induced by GdnHCl revealed unusual characteristics of the fluorescence of the single Trp 16 of this protein.

Analysis of the microenvironment of the single tryptophan residue of pOBP revealed that, though it is located in the macromolecule periphery (Figure 7A,B), the density of its microenvironment is rather high. In fact, it contains 80 atoms of amino acids and 3 molecules (131, 132, and 178) of bound water (d = 0.76). The shortest distance between the atoms of the water-bound molecules and the atoms of the indole ring is 4.13 between O132 and CZ2, 4.37 between O178 and NE1, and 6.13 Å O131 and CZ2. Interestingly, the most effective quencher of tryptophan residue fluorescence, the disulfide bond (Cys 63−Cys 155), is about 20 Å far from the indole ring, and this does not explain the lower quantum yield of pOBP in the native state in comparison with the

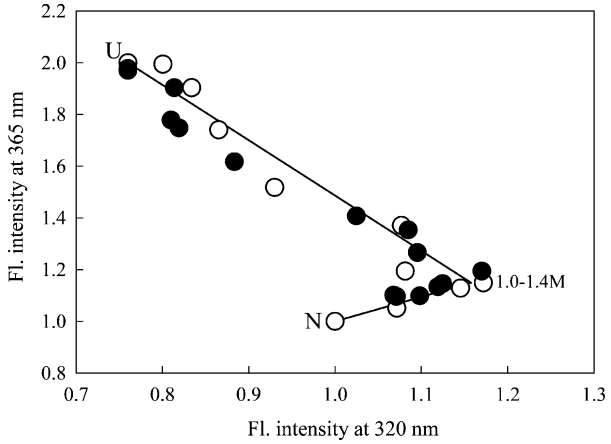

FIGURE 6: Parametric relationships between I_{320} and I_{365}, characterizing GdnHCl induced unfolding of pOBP. Closed circles represent the results of pOBP refolding. The values on the curves represent the values of GdnHCl concentrations. λ_{ex} = 297 nm.

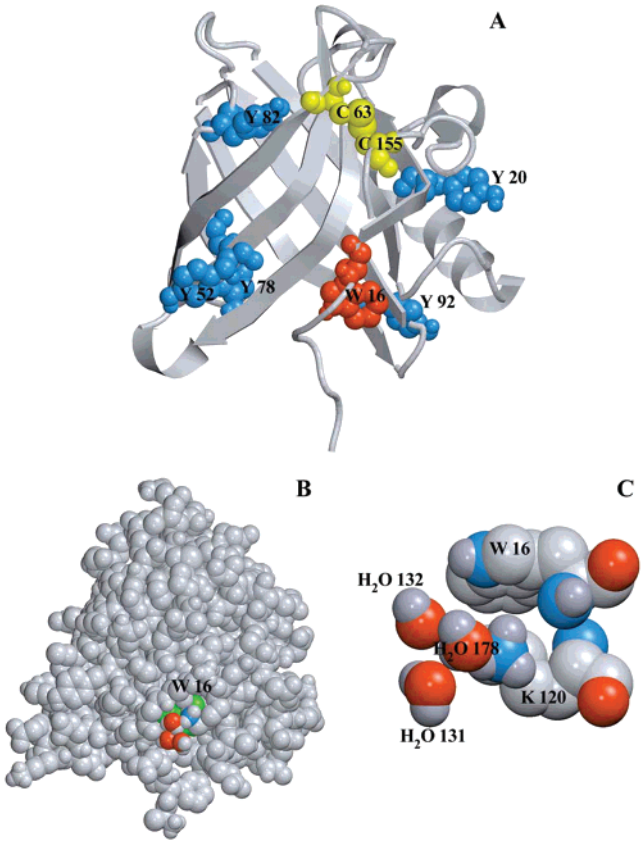

FIGURE 7: Spatial pattern of pOBP. (A) Cartoon diagram of the protein. Localization of Trp 16 residue (red), Tyr residues (blue), and the disulfide bridge made between Cys 63 and Cys 155 (yellow) are shown as spheres. (B) The surface of the protein. Trp16, NZ atom of Lys 120, and O atoms of bound water molecules 131, 132, and 178 are shown in green, blue, and red, respectively. (C) Spatial location of Trp 16, Lys 120, and bound water molecules 131, 132, 178 in the structure of pOBP. The figure is constructed on the basis of pOBP structure given in file 1A3Y.pdb (*9*). The drawing was generated by the graphic programs VMD and Raster 3D (*29*, *34*).

unfolded protein in 5.0 M GdnHCl. The absence of any aromatic ring in the vicinity of Trp 16 and the conformation of its side chain (Trp 16 is g$^+$-conformer χ_1 = 292°, χ_2 = 111°) can also be essential for its fluorescence characteristics (*35*, *36*). MD simulations did not reveal changes of Trp 16

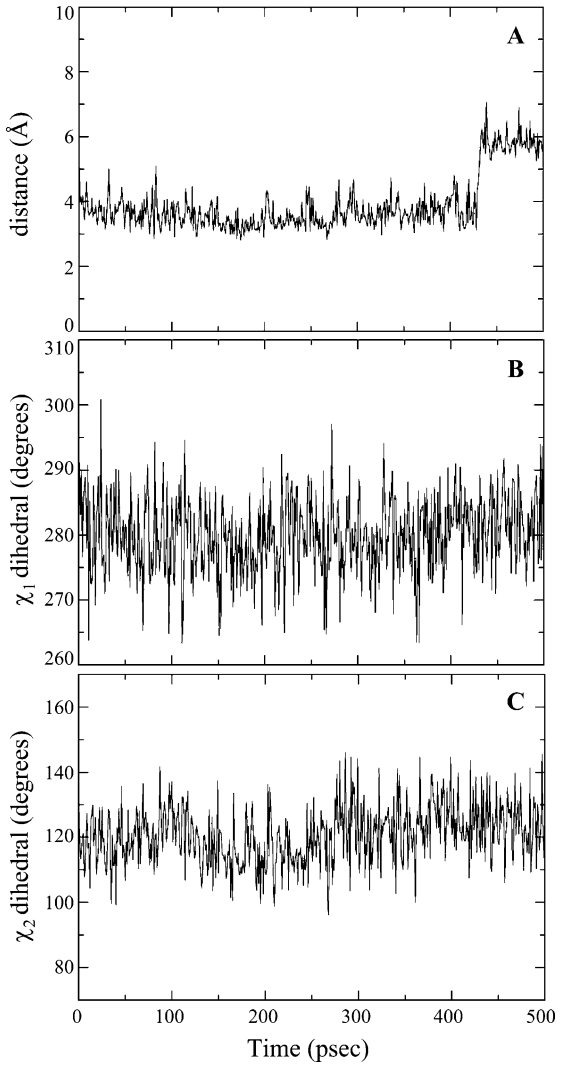

FIGURE 8: Time dependences of the distance between the NZ atom of Lys 120 and the indole ring of Trp 16 (panel A), and of dihedral angles χ_1 (panel B) and χ_2 (panel C).

side chain conformation (Figure 8). We suggested that Trp 16 fluorescence characteristics are to a great extent dependent on the positively charged NZ atom of Lys 120 located in its close vicinity.

The Role of Lys 120 and Bound Water in the Formation of Trp 16 Fluorescence Characteristics. The only polar group in the vicinity of Trp 16 is Lys 120 (Figure 7C). It has been shown that lysine residue is a weak quencher of tryptophan fluorescence (*37*). The side chain of Lys 120 is located practically parallel to the indole ring of Trp 16. The nearest atom of this residue NZ is separated from the center of the indole ring by only 4.15 Å. For this atom the nearest atoms of the indole ring are CE2 (4.24 Å), CZ2 (4.24 Å), and CH2 (4.3 Å). We have previously mentioned that quenching efficiency of polar groups depends not only on the distance between the quenching group and Trp residue but to a great extent upon its spatial location relative to the indole ring (*17*, *33*). Probably it is very important that positive charge of Lys 120 is located just over the center of the indole ring, since this charge location is known to be the most favorable for the formation of a complex between this group and the indole ring (*38*). Complex formation between Trp 16 and Lys 120 could explain the low fluorescence intensity of the native protein. It is necessary to keep in mind that in the

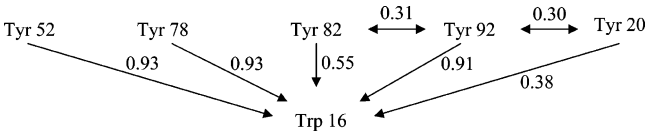

FIGURE 9: Efficiency of nonradiative energy transfer between tyrosine residues and from tyrosine residues to Trp 16 in pOBP.

vicinity of Trp 16 there are three molecules of bound water (see above) which also can make a complex with the indole ring in the ground and excited states.

On increasing of GdnHCl concentration, pOBP fluorescence intensity (quantum yield) raises, while fluorescence lifetime decreases. The possibility of absence of correlation between fluorescence lifetime $\langle\tau\rangle$ and fluorescence quantum yield $\langle q\rangle$ for tryptophan residues in proteins was for the first time mentioned by Szabo et al. (*39*). For several proteins with one tryptophan residue, it was found that the radiation lifetime $\tau_0 = \tau/q$ can differ. We have suggested that uncorrelated changes of fluorescence lifetime and quantum yield could be explained by the formation of exciplexes (*16*). The formation of such a complex was for example found for RNase T1 (*40*): it was shown that single Trp 59 of RNase T1 in the excited state forms a complex with the molecule of bound water located in the vicinity of the NE1 atom of the indole ring (*40*). So, the possibility that this can also happen with pOBP should not be excluded.

The addition of a small amount of GdnHCl (up to 1.4 M) does not change the tertiary structure of the protein; however, the tryptophan microenvironment is likely disturbed leading to disruption of the complex of Trp 16 with the NZ atom of Lys 120 and consequently to the enhancement of fluorescence intensity. The possibility of significant increase of the distance between atom NZ of Lys 120 and the indole ring of the tryptophan residue of pOBP in water was shown by molecular dynamic simulations (Figure 8). Apparently in 1.2 M GdnHCl such events will happen more frequently. Such tryptophan microenvironment disturbance does not change the accessibility of tryptophan residue to the solvent. It remains as low as in water (Figure 5). At the same time asymmetry of tryptophan residue microenvironment even increases (Figure 4, inset). This can also promote the formation of exciplexes of Trp 16 with bound water molecules, which like Lys 120 are in close vicinity to Trp 16 (Figure 7C) and can explain the decrease of fluorescence lifetime.

It is known that GdnHCl (like urea) is a better solvent for the unfolded state than for the folded state of proteins. GdnHCl is supposed to form hydrogen bonds with the polar groups of the polypeptide backbone thereby favoring the more solvent-exposed state. So, the further addition of GdnHCl from 1.4 to 3.5 M breaks down the tertiary structure and consequently disturbs the complex that Trp forms in the protein native state with Lys 120, thus inducing a further increase of fluorescence intensity and a red shift of fluorescence spectrum.

Besides Trp 16, pOBP also possesses five tyrosine residues whose contribution to the intrinsic fluorescence of the protein upon excitation at 280 nm is quite small (Figure 2B). This can be explained by an effective energy transfer from tyrosine residues to Trp 16 (Figure 9). As it could be expected, in the unfolded protein the conditions for an effective energy transfer are disturbed and consequently, when the protein is

denatured by GdnHCl, the contribution of the tyrosine residues to the bulk fluorescence of pOBP increases significantly (Figure 2C). In the unfolded protein, the tyrosine fluorescence emission spectrum becomes distinctly separated from that of the tryptophan residue, which is red-shifted (Figure 2B). As it was mentioned in the previous section, the change of fluorescence intensity (quantum yield) and fluorescence lifetime in the range of 0.0−1.4 M GdnHCl are caused by the local changes in the microenvironment of the tryptophan residue, but not by a global change of protein structure.

Stability of pOBP Structure to Denaturating Action of GdnHCl. The nature of the changes of all other fluorescence parameters and that of CD spectra suggests that the unfolding process starts at higher concentration of GdnHCl (1.4−3.5 M) and that it is a two-state reversible process, at least at a temperature between 20 and 25 °C. Analysis allows the determination of thermodynamic parameters describing protein stability to the denaturating action of GdnHCl. Usually it is taken that protein stability (*i.e.*, the difference between protein free energy in native and unfolded states) is a linear function of denaturant concentration (*41*):

$$\Delta G^\circ([\mathrm{D}]) = \Delta G^\circ([0]) + m[\mathrm{D}] \quad (6)$$

where [D] is concentration of denaturant, $\Delta G^\circ([0])$ is the difference of free energy of macromolecule in the absence of denaturant, $m = \mathrm{d}(\Delta G_{\mathrm{N-U}}[\mathrm{D}])/\mathrm{d}([\mathrm{D}])$. The value $\Delta G([\mathrm{D}])$ is connected with the equilibrium constant $K_{\mathrm{N-U}}$ by equation

$$\Delta G^\circ_{\mathrm{N-U}}([\mathrm{D}]) = \Delta H^\circ_{\mathrm{N-U}}([\mathrm{D}]) - T\Delta S^\circ_{\mathrm{N-U}}([\mathrm{D}]) = -RT \ln K_{\mathrm{N-U}}([\mathrm{D}]) \quad (7)$$

where H is enthalpy, T is the absolute temperature, S is entropy, and R is the universal gas constant. For any extensive characteristic of the system containing two components, *e.g.*, for fluorescence intensity, we can write

$$I([\mathrm{D}]) = \alpha_{\mathrm{N}}([\mathrm{D}])I_{\mathrm{N}} + \alpha_{\mathrm{U}}([\mathrm{D}])I_{\mathrm{U}} \quad (8)$$

$$\alpha_{\mathrm{N}}([\mathrm{D}]) + \alpha_{\mathrm{U}}([\mathrm{D}]) = 1$$

consequently,

$$K([\mathrm{D}]) = \frac{I_{\mathrm{N}} - I([\mathrm{D}])}{I([\mathrm{D}]) - I_{\mathrm{U}}} \quad (9)$$

It must be pointed out that this simple equation for determining $K([\mathrm{D}])$ is valid only for the extensive characteristics of systems, and not for the intensive ones, such as parameter A, and fluorescence anisotropy. At the same time often it is not considered and even the position of fluorescence spectrum maximum is used for determination of equilibrium constant (*42*). To illustrate the statement that eq 9 is valid only for extensive values, we shall show how parameter A is connected with the equilibrium constant $K([\mathrm{D}])$ between the N and U states. By assuming that parameter A can be presented as follows,

$$A = \frac{I_{320}([\mathrm{D}])}{I_{365}([\mathrm{D}])} = \frac{\alpha_{\mathrm{N}}I_{\mathrm{N},320}([\mathrm{D}]) + \alpha_{\mathrm{U}}I_{\mathrm{U},320}([\mathrm{D}])}{\alpha_{\mathrm{N}}I_{\mathrm{N},365}([\mathrm{D}]) + \alpha_{\mathrm{U}}I_{\mathrm{U},365}([\mathrm{D}])} \quad (10)$$

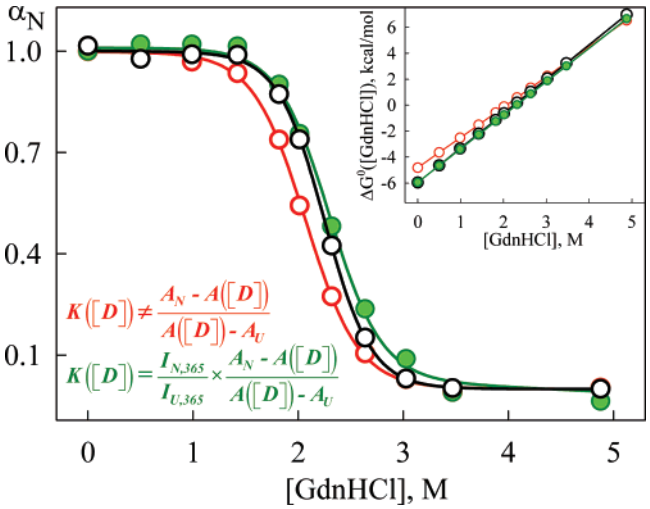

FIGURE 10: The determination of thermodynamic characteristics of pOBP unfolding by GdnHCl. The dependences of part of native pOBP molecules (α_{N}) on GdnHCl concentration determined on the basis of the ellipticity at 222 nm (black symbols) and on the basis of parameter A taking into account correction coefficient ($I_{\mathrm{N},365}/I_{\mathrm{U},365}$) (green symbols) and regardless of it (red symbols). Inset: The corresponding dependences of ΔG° on the GdnHCl concentration.

it will be easy to show that

$$K([\mathrm{D}]) = \frac{I_{\mathrm{N},365}}{I_{\mathrm{U},365}} \frac{A_{\mathrm{N}} - A([\mathrm{D}])}{A([\mathrm{D}]) - A_{\mathrm{U}}} \quad (11)$$

Evidently, eq 11 is similar to eq 9, but they differ by the coefficient $I_{\mathrm{N},365}/I_{\mathrm{U},365}$. So parameter A cannot be used for the evaluation of the equilibrium constant without correction of the coefficient and for certain maximum of fluorescence spectrum position cannot be used for the determination of the value of the equilibrium constant.

In conclusion, with the use of intrinsic fluorescence and CD methods, in the present study we have shown that pOBP unfolding induced by GdnHCl is a one-stage reversible process. Data were used for the determination of thermodynamic characteristics of pOBP unfolding by GdnHCl (Figure 10). The midpoint of the transition, where the free energies of the protein in native and unfolded states are equal, corresponds to 2.3 M of GdnHCl, $m = 2.6$ kcal mol^{-1} M^{-1}. The difference of protein free energy in the native and unfolded states in the absence of denaturant is −5.95 kcal/mol, *i.e.*, protein is very stable to the denaturating action of GdnHCl.

ACKNOWLEDGMENT

We gratefully acknowledge Dr. Umberto Amato for the availability of the cluster “Lilligrid” located at the IAC-CNR, Naples, to run MD simulations with the program GROMACS.

REFERENCES

1. Flower, D. R., North, A. C., and Sansom, C. E. (2000) The lipocalin protein family: structural and sequence overview, *Biochim. Biophys. Acta 1482*, 9−24.
2. Nygren, P. A., and Skerra, A. (2004) Binding proteins from alternative scaffolds, *J. Immunol. Methods 290*, 3−28.
3. Skerra, A. (2000) Lipocalins as a scaffold, *Biochim. Biophys. Acta 1482*, 337−350.

4. Schlehuber, S., and Skerra, A. (2005) Lipocalins in drug discovery: from natural ligand-binding proteins to "anticalins", *Drug Discovery Today 10*, 23−33.
5. Korndorfer, I. P., Schlehuber, S., and Skerra, A. (2003) Structural mechanism of specific ligand recognition by a lipocalin tailored for the complexation of digoxigenin, *J. Mol. Biol. 330*, 385−396.
6. Tegoni, M., Pelosi, P., Vincent, F., Spinelli, S., Campanacci, V., Grolli, S., Ramoni, R., and Cambillau, C. (2000) Mammalian odorant binding proteins, *Biochim. Biophys. Acta 1482*, 229−240.
7. Tegoni, M., Ramoni, R., Bignetti, E., Spinelli, S., and Cambillau, C. (1996) Domain swapping creates a third putative combining site in bovine odorant binding protein dimer, *Nat. Struct. Biol. 3*, 863−867.
8. Bianchet, M. A., Bains, G., Pelosi, P., Pevsner, J., Snyder, S. H., Monaco, H. L., and Amzel, L. M. (1996) The three-dimensional structure of bovine odorant binding protein and its mechanism of odor recognition, *Nat. Struct. Biol. 3*, 934−939.
9. Spinelli, S., Ramoni, R., Grolli, S., Bonicel, J., Cambillau, C., and Tegoni, M. (1998) The structure of the monomeric porcine odorant binding protein sheds light on the domain swapping mechanism, *Biochemistry 37*, 7913−7918.
10. Dal Monte, M., Andreini, I., Revoltella, R., and Pelosi, P. (1991) Purification and characterization of two odorant-binding proteins from nasal tissue of rabbit and pig, *Comp. Biochem. Physiol. B 99*, 445−451.
11. Turoverov, K. K., Biktashev, A. G., Dorofeiuk, A. V., and Kuznetsova, I. M. (1998) A complex of apparatus and programs for the measurement of spectral, polarization and kinetic characteristics of fluorescence in solution, *Tsitologiia 40*, 806−817.
12. Turoverov, K. K., and Kuznetsova, I. M. (2003) Intrinsic fluorescence of actin, *J. Fluoresc. 13*, 41−57.
13. Marquardt, D. W. (1963) An algorithm for least-squares estimation of nonlinear parameters, *J. Soc. Ind. Appl. Math. 11*, 431−441.
14. Eftink, M. R. (1991) Fluorescence quenching: theory and applications, in *Topics in fluorescence spectroscopy* (Lakowicz, J. R., Ed.) Vol. 2, pp 53−120, Plenum Press, New York and London.
15. Berman, H., Henrick, K., Nakamura, H., and Markley, J. L. (2007) The worldwide Protein Data Bank (wwPDB): ensuring a single, uniform archive of PDB data, *Nucleic Acids Res. 35*, D301−D303.
16. Turoverov, K. K., Kuznetsova, I. M., and Zaitsev, V. N. (1985) The environment of the tryptophan residue in *Pseudomonas aeruginosa* azurin and its fluorescence properties, *Biophys. Chem. 23*, 79−89.
17. Kuznetsova, I. M., and Turoverov, K. K. (1998) What determines the characteristics of the intrinsic UV-fluorescence of proteins? Analysis of the properties of the microenvironment and features of the localization of their tryptophan residues, *Tsitologiia 40*, 747−762.
18. Forster, Th. (1960) Transfer mechanisms of electronic excitation energy, *Rad. Res. Suppl. 2*, 326−339.
19. Dale, R. E., and Eisinger, J. (1974) Intramolecular distances determined by energy transfer. Dependence on orientational freedom of donor and acceptor, *Biopolymers 13*, 1573−1605.
20. Eisinger, J., Feuer, B., and Lamola, A. A. (1969) Intramolecular singlet excitation transfer. Applications to polypeptides, *Biochemistry 8*, 3908−3915.
21. Lindahl, E., Hess, B., and van der Spoel, D. (2001) GROMACS 3.0: a package for molecular simulation and trajectory analysis, *J. Mol. Model. 7*, 306−317.
22. van der Spoel, D., Lindahl, E., Hess, B., Groenhof, G., Mark, A. E., and Berendsen, H. J. C.(2005) GROMACS: Fast, Flexible and Free, *J. Comput. Chem. 26*, 1701−1718.
23. Jorgensen, W. L., Maxwell, S., and Tirado-Rives, J. (1996) Development and testing of the OPLS All-Atom Force Field on conformational energetics and properties of organic liquids, *J. Am. Chem. Soc. 118*, 11225−11236.
24. Kaminski, G. A., Friesner, R. A., Tirado-Rives, J., and Jorgensen, W. L. (2001) Evaluation and reparametrization of the OPLS-AA Force Field for proteins via comparison with accurate quantum chemical calculations on peptides, *J. Phys. Chem. B 105*, 6474−6487.
25. Berendsen, H. J. C., Postma, J. P. M., van Gunsteren, W. F., and Hermans, J. (1981) in *Intermolecular Forces* (Pullman, B., Ed.) p 331, D. Reidel Publishing Company, Dordrecht.
26. Hess, B., Bekker, H., Berendsen, H. J. C., and Fraaije, J. G. E. M. (1997) LINCS: A linear constraint solver for molecular simulations, *J. Comput. Chem. 18*, 1463−1472.
27. Berendsen, H. J. C., Postma, J. P. M., Di Nola, A., and Haak, J. R. (1984) MD with coupling to an external bath, *J. Phys. Chem. 81*, 3684−3690.
28. Essmann, U., Perera, L., Berkowitz, M. L., Darden, T., Lee, H., and Pedersen, L. G. (1995) A smooth particle mesh Ewald method, *J. Chem. Phys. 103*, 8577−8593.
29. Humphrey, W., Dalke, A., and Schulten, K. (1996) VMD: Visual Molecular Dynamics, *J. Mol. Graphics 14*, 33−38.
30. Grinvald, A., and Steinberg, I. Z. (1976) The fluorescence decay of tryptophan residues in native and denatured proteins, *Biochim. Biophys. Acta 427*, 663−678.
31. Stepanenko, O. V., Marabotti, A., Kuznetsova, I. M., Turoverov, K. K., Fini, C., Varriale, A., Staiano, M., Rossi, M., and D'Auria, S. Hydrophobic interactions and ionic networks play an important role in thermal stability and denaturation mechanism of the porcine odorant binding protein, *Proteins*, in press.
32. Kuznetsova, I. M., Turoverov, K. K., and Uversky, V. N. (2004) Use of the phase diagram method to analyze the protein unfolding-refolding reactions: fishing out the "invisible" intermediates, *J. Proteome Res. 3*, 485−494.
33. D'Auria, S., Staiano, M., Kuznetsova, I. M., and Turoverov, K. K. (2005) The combined use of fluorescence spectroscopy and X-ray crystallography greatly contributes to elucidating structure and dynamics of proteins, *Rev. Fluoresc.* 25−61.
34. Merritt, E. A., and Bacon, D. J. (1977) Raster 3-D: Photorealistic molecular graphics, *Methods Enzymol. 277*, 505−524.
35. Pan, C. P., Barkley, M. D. (2004) Conformational effects on tryptophan fluorescence in cyclic hexapeptides, *Biophys. J. 86*, 3828−3835.
36. Pan, C. P., Callis, P. R., and Barkley, M. D. (2006) Dependence of tryptophan emission wavelength on conformation in cyclic hexapeptides, *J. Phys. Chem. B. 110*, 7009−7016.
37. Chen, Y., and Barkley, M. D. (1998) Toward understanding tryptophan fluorescence in proteins, *Biochemistry 37*, 9976−9982.
38. Vivian, J. T., and Callis, P. R. (2001) Mechanisms of tryptophan fluorescence shifts in proteins, *Biophys. J. 80*, 2093−2109.
39. Szabo, A. G., and Faerman, C. (1992) Dilemma of correlating fluorescence quantum yields and intensity decay times in single-tryptophan mutant proteins, *Proc. SPIE 1640*, 70−80.
40. Axelsen, P. H., and Prendergast, F. G. (1989) Molecular dynamics of tryptophan in ribonuclease-T1. II. Correlations with fluorescence, *Biophys. J. 56*, 43−66.
41. Nolting, B. (1999) Protein Folding Kinetics, in *Biophysical Methods*, p 145, Springer-Verlag, Berlin-Heidelberg.
42. Parisi, M., Mazzini, A., Sorbi, R. T., Ramoni, R., Grolli, S., and Favilla, R. (2003) Unfolding and refolding of porcine odorant binding protein in guanidinium hydrochloride: equilibrium studies at neutral pH, *Biochim. Biophys. Acta 1652*, 115−125.

BI7008129